High-frequency ultrasound signal detection using light

Ayan Majumder

A dissertation submitted for the partial fulfillment of BS-MS dual degree in Science

Indian Institute of Science Education and Research Mohali

April 2019

Certificate of Examination

This is to certify that the dissertation titled "High-frequency ultrasound signal detection using light" submitted by Mr. Ayan Majumder (Reg. No. MS14103) for the partial fulfillment of BS-MS dual degree program of the Institute, has been examined by the thesis committee duly appointed by the Institute. The committee finds the work done by the candidate satisfactory and recommends that the report be accepted.

Dr. Ananth Venkatesan Dr. Sandeep Kumar Goyal Dr. Samir Kumar Biswas

(Supervisor)

Dated: April 25, 2019

Declaration

The work in this dissertation has been carried out by me under the guidance of Dr. Samir Kumar Biswas at the Indian Institute of Science Education and Research Mohali.

This work has not been submitted in part or in full for a degree, a diploma, or a fellowship to any other university or institute. Whenever contributions of others are involved, every effort is made to indicate this clearly, with due acknowledgement of collaborative research and discussions. This thesis is a bonafide record of original work done by me and all sources listed within have been detailed in the bibliography.

Ayan Majumder

(Candidate)

Dated: April 25, 2019

In my capacity as the supervisor of the candidate's project work, I certify that the above statements by the candidate are true to the best of my knowledge.

Dr. Samir Kumar Biswas

(Supervisor)

Acknowledgement

My deepest gratitude is to my advisor, *Dr. Samir Kumar Biswas*. I have been amazingly fortunate to have an advisor who gave me the freedom to explore on my own, and at the same time gave the guidance to recover when my steps faltered. His patience and support helped me to overcome many crisis situations and finish this thesis work.

I want to thank *Dr. Ananth Venkatesan* and *Dr. Sandeep Kumar Goyal* for useful discussion about the thesis work.

I also want to thank my parents, brother and friends for their constant support and inspiration.

Ayan Majumder

List of Figures

1.1 Schematic diagram of photo-acoustic signal generation. 1

2.1 High frequency signal detection using optical methods(reference-(WPRN18)). 4

2.2 Comparison between the material based sensors and the optics based sensor(reference-(WPRN18)). 4

2.3 Schematic diagram of the Mach-Zehnder interferometer. 6

2.4 Experimental setup of the Mach-Zehnder interferometer. 6

2.5 Inteference pattarn at the detector-0. Where we consider R=T. . . . 8

2.6 Inteference pattarn at the detector-1. Where we consider R=T. . . . 8

2.7 Schematic diagram of the ultrasound detection using MZI. 9

2.8 Experimental setup of the ultrasound detection using MZI. 9

2.9 Detection of ultrasound by the deflection of a laser beam(reference-(MIR$^+$16)) 10

2.10 Schematic diagram of the interaction of probe beam and the ultrasound wave(reference-(MIR$^+$16)). 10

2.11 Schematic diagram of the inline Mach-Zehnder interferometer. 12

2.12 High frequency signal detection using optical methods. 12

2.13 Schematic diagram of the interference formation. 13

2.14 (a) Reflected ultrasound signal. (b) Intensity distribution due to the interference. (c)After reducing the beam width using 500μm pinhole, only reflected ultrasound signal is there. 15

3.1 Schematic diagram of the optical fiber based Mach-Zehnder interferometer. 17

3.2 Micro-cavity on the optical fiber. 17

4.1 Electric-arc based micro-machining system. 19
4.2 Different kind of optical fiber holders of the micro-machining system. 19
4.3 Procedure of cavity preparation. 20
4.4 Micro-spheres using micro-machining system. 20

Contents

List of Figures **i**

Abstract **iii**

1 Introduction **1**

2 High-frequency signal detection using optical methods **3**

2.1 Free space Mach-Zehnder interferometer 5

2.2 Detection of ultrasound by the deflection of a laser beam 10

2.3 Ultrasound detection using inline Mach-Zehnder interferometer 11

3 Optical fiber based Mach-Zehnder interferometer **16**

4 Electric-arc based micro-machining system **18**

5 Future plans **21**

Abstract

Nowadays people are interested in the photoacoustic microscopy to study biological samples(Like, tissues). In such kind of studies, there is no need to take samples(cells or tissues) out from the living being. Generally, people use material based sensors to detect the photoacoustic signals. But there are lots of limitations (i.e. lack of large bandwidth, small size, sensitivity, high-frequency sensing) in such kind of sensors. Besides these reasons, material based sensors are easily affected by the environment(i.e. temperature, electromagnetic interference). So, there is a high probability to get noisy signals. Due to those reasons, people are interested to develop optics based high-frequency photoacoustic sensor. Here, we have used the Mach-Zehnder interferometric technique and the beam deflectometry technique to detect the MHz range high-frequency ultrasound signal. We have also proposed a new experimental setup to detect the ultrasound signal using inline Mach-Zehnder interferometer with a single wide beam. In this proposed setup, we have observed interference and the beam deflection due to the ultrasound wave simultaneously. Besides this, we have also described some optical fiber based sensor fabrication which can able to detect the ultrasound signals.

Chapter 1

Introduction

Our actual aim is to detect the high-frequency photoacoustic signals. Photoacoustic signals are generated from the biological tissues and some other materials. Biological cells and some other materials absorb the photons(emitted from NIR laser) for a very short time, that energy generates heat inside that material, so some local thermo-elastic expansion will happen inside that material. After that, these materials try to release that energy, so contraction will happen. Due to the expansion and contraction, some sound wave will generate inside that material. Such kind of sound waves is known as photo-acoustic waves. The whole process is shown schematically in the Figure 1.1.

Here, we are interested in the photo-acoustic signals which are generated from the biological tissues. We can reconstruct the image of the biological cells from these

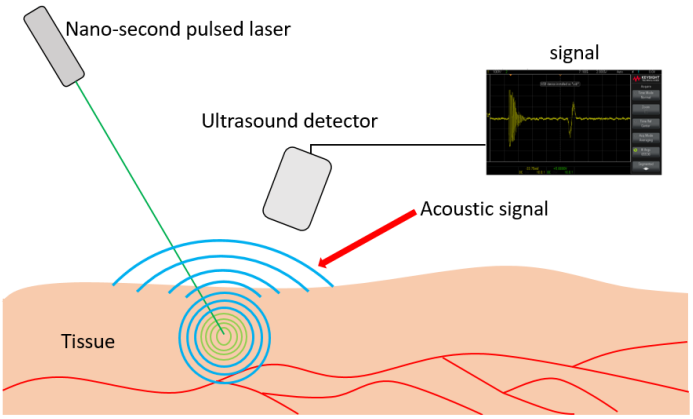

Figure 1.1: Schematic diagram of photo-acoustic signal generation.

photoacoustic signals. Generally, people use piezoelectric transducers(PZTs) to detect such kind of ultrasonic signals. Those sensors are based on thin piezoelectric polymer film(polyvinylidene fluoride), are wideband and highly sensitive. However, the sensitivity of those sensors decreases as their size is reduced. Due to this problem at high ultrasonic frequencies when the detector size should be shorter than half of the wavelength of the signal or when the sensor needs to be miniaturized for integration in an array of sensors. Another drawback of piezoelectric sensors is that they create electrical signals which are easily affected by the environment. Due to those limitations, the optical detection of ultrasound for biomedical applications has been studied as an alternative to piezoelectric technology for decades. Here, we are going to discuss the ultrasound detection using optical methods.

Chapter 2

High-frequency signal detection using optical methods

In the introduction part, we already describe the limitations of the material based sensors. So, nowadays people are focusing on optics based sensors to make more compact, low noise, and more sensitive sensors. According to the reference-(WPRN18), people already detected ultrasound signals using various optical methods. There is a detailed analysis of the material based and optically based acoustic sensor development in reference-(WPRN18), where they are presented major four design with laser light for detection ultrasound signals(see Figure-2.1).

Here, we are going to describe some of the optics based sensors briefly. There are two optical methods to detect the ultrasound wave. One is **refractometry** and other one is **interferometry**.In the refractometry based optical detection, the photo-elastic principle is used. According to this principle, when the acoustic waves interact with the medium, it induces mechanical stress in the medium. Due to this mechanical stress refractive index modulation is happened inside the medium. In this method, there is a laser beam(called probe beam) to measure the refractive index modulation of the medium. In this case, people generally measure the overall intensity variation, deflection angle or phase of the probe beam to get the actual information of the acoustic waves. In the interferometry technique, there will be a reference beam and an object beam. When acoustic wave passing through the medium it will modulate the refractive index of the medium and the object beam will be affected by that

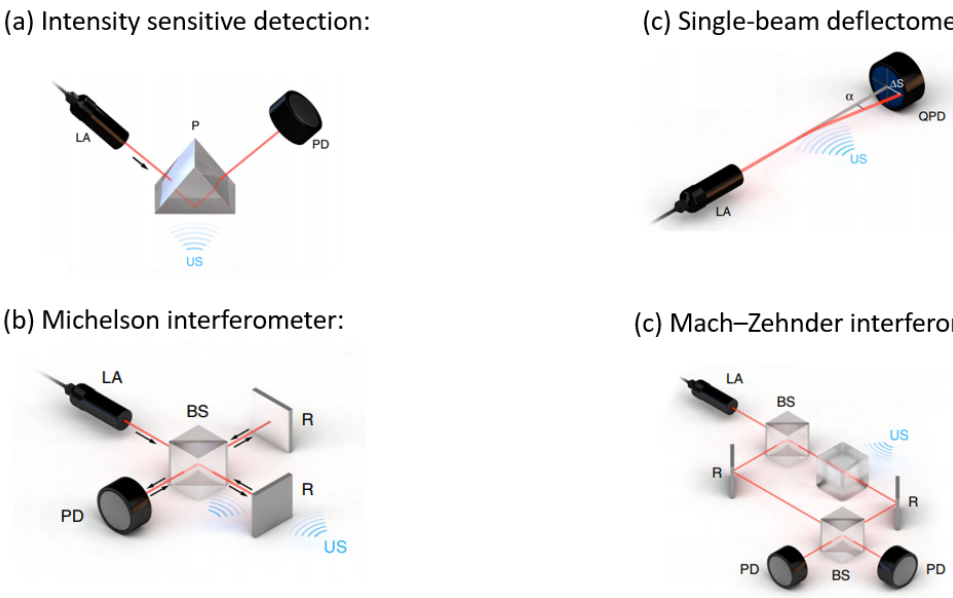

Figure 2.1: High frequency signal detection using optical methods(reference-(WPRN18)).

Refractometric transducer	**Material**	**Read-out element**	**Bandwidth (MHz)**	**Sensing element size (mm)**	**NEP (mPa/Hz$^{1/2}$)**	**NEP × area (mPa mm^2/Hz$^{1/2}$)**
Intensity-sensitive	Silica	Photodiode	100	Prism (15)	100	22×10^3
Beam deflectometry	Coupling medium	QPD	17	Needle beam (0.09)	2.76	N.A.
Phase-sensitive	Coupling medium	CCD/CMOS	110	Schlieren beam (10)	486	N.A.
Interferometric transducer	**Material**	**Dimensions (H × W × L, µm)**	**Q-factor**	**Conversion efficiency (M/Pa)$^{-1}$**	**NEP (mPa/Hz$^{1/2}$)**	**NEP × area (mPa mm^2/Hz$^{1/2}$)**
Micro-ring	Polystyrene	$1.4 \times 20 \times 20$ —$1.4 \times 100 \times 100$	1.4×10^5	130×10^{-6}	5.61	1.8×10^{-3}
Fabry-Pérot	PET/Parylene C	$38 \times 90 \times 90$	2.8×10^3	90×10^{-6}	78	0.63
	SU8	$10 \times 15 \times 15$	300	N.R.	200	4.5×10^{-2}
	Fluid with low optical absorption	$60 \times 60 \times 2 \times 10^3$	N.R.	N.R.	0.45	5.4×10^{-2}
π-BG	Silica	$10 \times 10 \times 270$	1.2×10^6	3.8×10^{-6}	25	6.75×10^{-2}
	Silicon	$0.2 \times 0.5 \times 30$	1.2×10^5	N.R.	N.R.	N.R.
Piezoelectric transducer	**Model**	**Detector type**	***f* (MHz)**	**Area (mm^2)**	**NEP (mPa/Hz$^{1/2}$)**	**NEP × area (mPA·mm^2/Hz$^{1/2}$)**
Olympus NDT panametrics	V214-BB-RM	Spherically focused piezoceramic	50	30	0.2	6
Precision acoustics	Needle (1 mm)	PVdF needle hydrophone	12	1	14.4	14.4
Boston Scientific	Atlantis PV	Intravascular ultrasound probe	15	0.8	450	360
Micromachined transducer	**Material**	**Detector type**	***f* (MHz)**	**Area (mm^2)**	**NEP (mPa/Hz$^{1/2}$)**	**NEP × area (mPA·mm^2/Hz$^{1/2}$)**
CMUT	Silicon	Array of capacitor cells	5	0.06	1.8	0.11

NEP noise equivalent pressure, *QPD* quadrant photodiode, *CCD* charge-coupled device, *CMOS* complementary metal-oxide-semiconductor, *PET* polyethylene terephthalate, *SU8* epoxy-based photoresist, *π-BG* pi-phase-shifted Bragg grating, *CMUT* capacitative micromachined ultrasonic transducer, *N.A.* not applicable, *N.R.* not reported

Figure 2.2: Comparison between the material based sensors and the optics based sensor(reference-(WPRN18)).

refractive index modulation. So, the optical path difference will be changed between the reference beam and the object beam. Due to this reason, the fringe shift happens in the interference pattern. From this fringe shift, we can find out the refractive index modulation of the medium. Using all this information we can reconstruct the acoustic signal. In Figure-2.1, some optics based ultrasound detection setups are shown.

2.1 Free space Mach-Zehnder interferometer

In the Mach-Zehnder interferometer(MZI), there is a 50:50 beam splitter(50:50 BS) which splits the incoming beam into two beams with 50-50 intensity. According to Figure 2.3, the input beam is denoted by the (1) and the output beams of the 50:50 BS are (3) and (4). After that, the beams (3) and (4) are reflected by the mirror 3 and mirror 4 respectively. Finally, those reflected beams are combined by the another 50:50 BS. Due to the superposition of these two beams, we can observe an interference pattern at the output of the 50:50 BS. In Figure 2.4, the MZI setup and the interference pattern are shown.

From Figure-2.3, we can illustrate the optical path difference between the two rays= $\delta L = [OM_4O'] - [OM_3O']$. Let, the electric field of the beam (1) is $E_1(O)$. The reflection and the transmission coefficient of the 50:50 BS are r and t respectively. Therefore, the equations of the beam (3) and beam (4) are given below,

$$E_3(O) = rE_1(O) \tag{2.1}$$

$$E_4(O) = tE_1(O) \tag{2.2}$$

Let, the optical path length of the reference and the object beam are L_3 and L_4 respectively. So the equations of these two beams at the second 50:50 BS are,

$$E_3(O') = e^{ikL_3}E_3(O) \tag{2.3}$$

$$E_4(O') = e^{ikL_4}E_4(O) \tag{2.4}$$

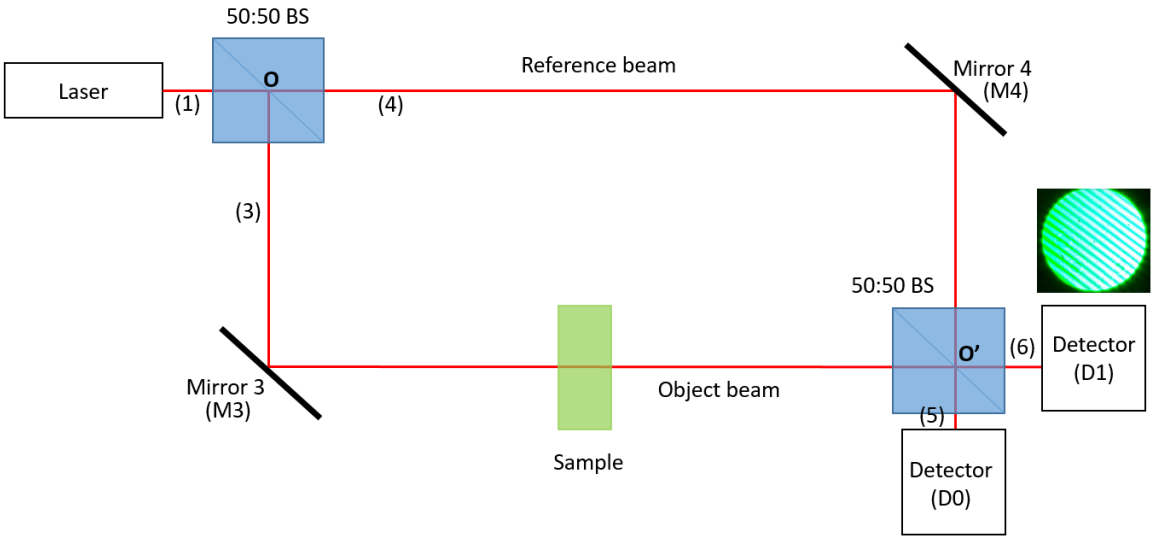

Figure 2.3: Schematic diagram of the Mach-Zehnder interferometer.

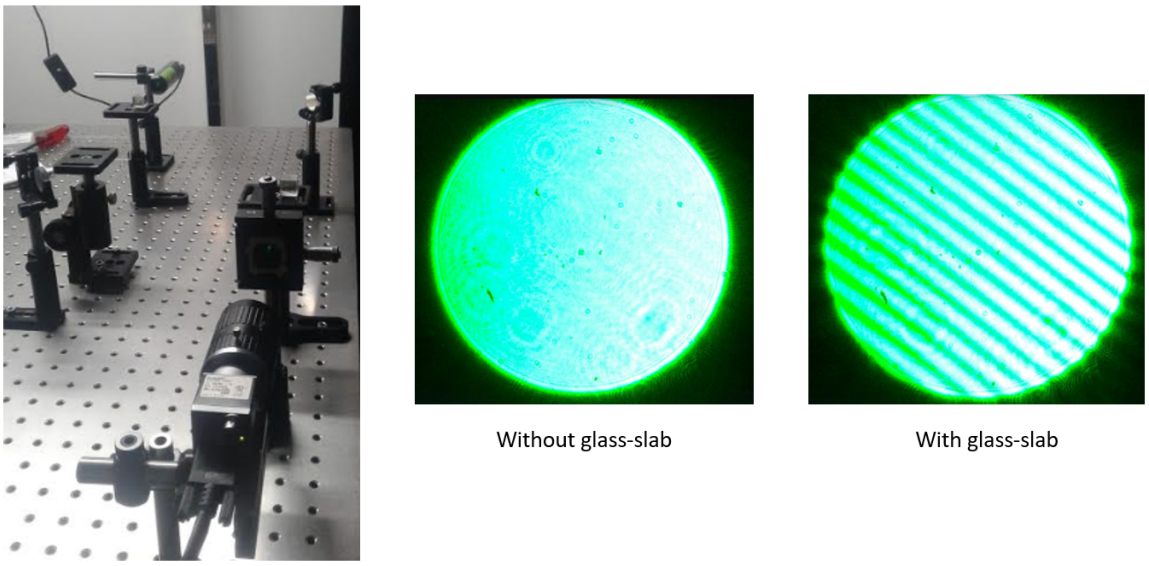

Figure 2.4: Experimental setup of the Mach-Zehnder interferometer.

Therefore, after the 50:50 BS the equations of the beam (5) and beam (6) will be,

$$E_5 = -rE_3(O') + tE_4(O') = -r^2 e^{ikL_3} E_1(O) + t^2 e^{ikL_4} E_1(O) \tag{2.5}$$

$$E_6 = rE_4(O') + tE_3(O') = rte^{ikL_3} E_1(O) + tre^{ikL_4} E_1(O) \tag{2.6}$$

Therefore,

$$|E_5|^2 = |-r^2 e^{ikL_3} E_1(O) + t^2 e^{ikL_4} E_1(O)|^2$$

$$\Rightarrow |E_5|^2 = |E_1(O)|^2[-Re^{ikL_3} + Te^{ikL_4}][-Re^{-ikL_3} + Te^{-ikL_4}]$$

$$\Rightarrow |E_5|^2 = |E_1(O)|^2[R^2 + T^2 - RT(e^{ik(L_3-L_4)} + e^{-ik(L_3-L_4)})]$$

$$\Rightarrow |E_5|^2 = |E_1(O)|^2(R^2 + T^2)[1 - \frac{RT}{R^2+T^2}(e^{ik(L_3-L_4)} + e^{-ik(L_3-L_4)})] \tag{2.7}$$

From eq-(7), we may say that the intensity distribution at the D0 is given below:

Similar way, we can write the intensity distribution function for the D0 is given below;

$$|E_6|^2 = |E_1(O)|^2(R^2 + T^2)[1 + \frac{RT}{R^2+T^2}(e^{ik(L_3-L_4)} + e^{-ik(L_3-L_4)})] \tag{2.8}$$

From eq-(2.8), we may say that the intensity distribution at the D1 is given below:

Now, if we introduce a glass slab or some optically transparent sample at the object arm, the optical path length change happens between the reference and object beam. The optical path length change is happened due to the refractive index of the sample. So the fringe shift will happen at the interference pattern. From this fringe shift, we can calculate the refractive index of the sample. Here, we have introduced ultrasound at the object arm to observe the fringe shift. When ultrasound propagates through the medium particles are shifted from there actual position and create denser and rarer medium along the ultrasound propagation path. Due to this phenomena, the object arm also faces the different refractive index. So, at the output, there is a possibility to get the fringe shift. The schematic diagram and the experimental setup of this kind of experiment are given in Figure-2.7 and 2.8.

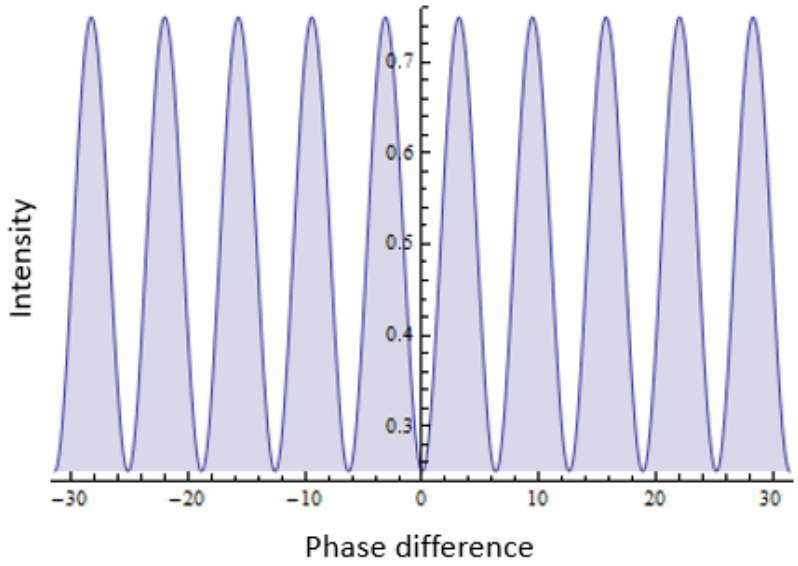

Figure 2.5: Inteference pattarn at the detector-0. Where we consider R=T.

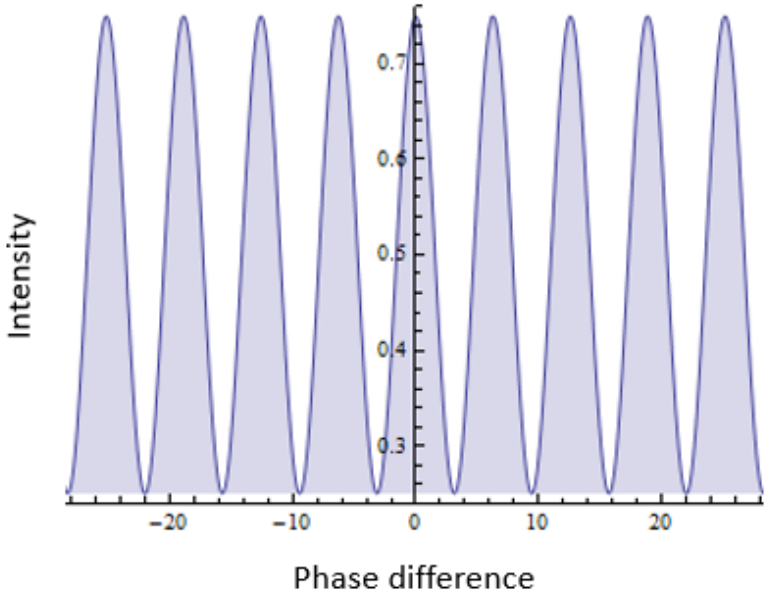

Figure 2.6: Inteference pattarn at the detector-1. Where we consider R=T.

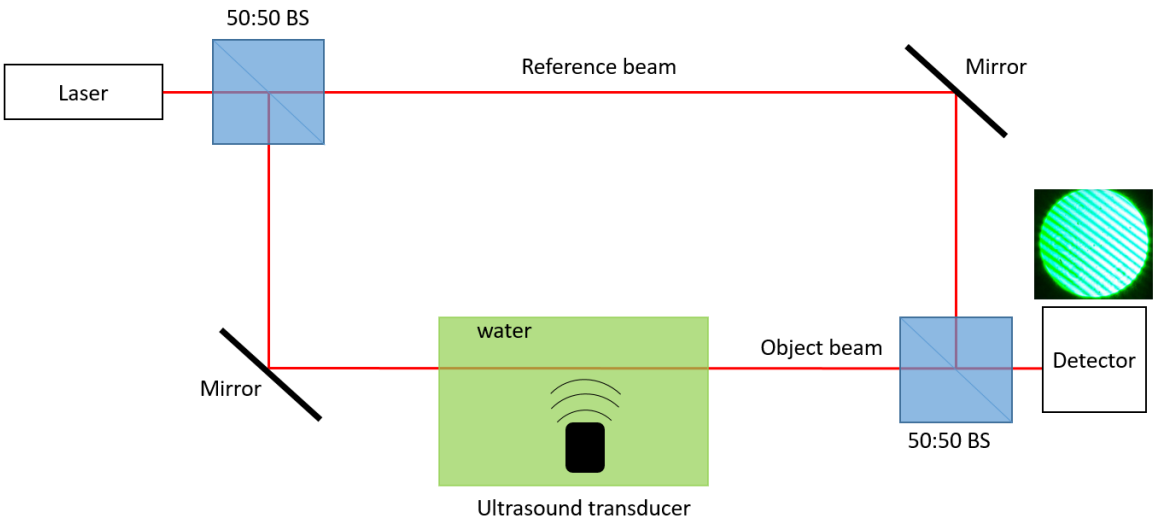

Figure 2.7: Schematic diagram of the ultrasound detection using MZI.

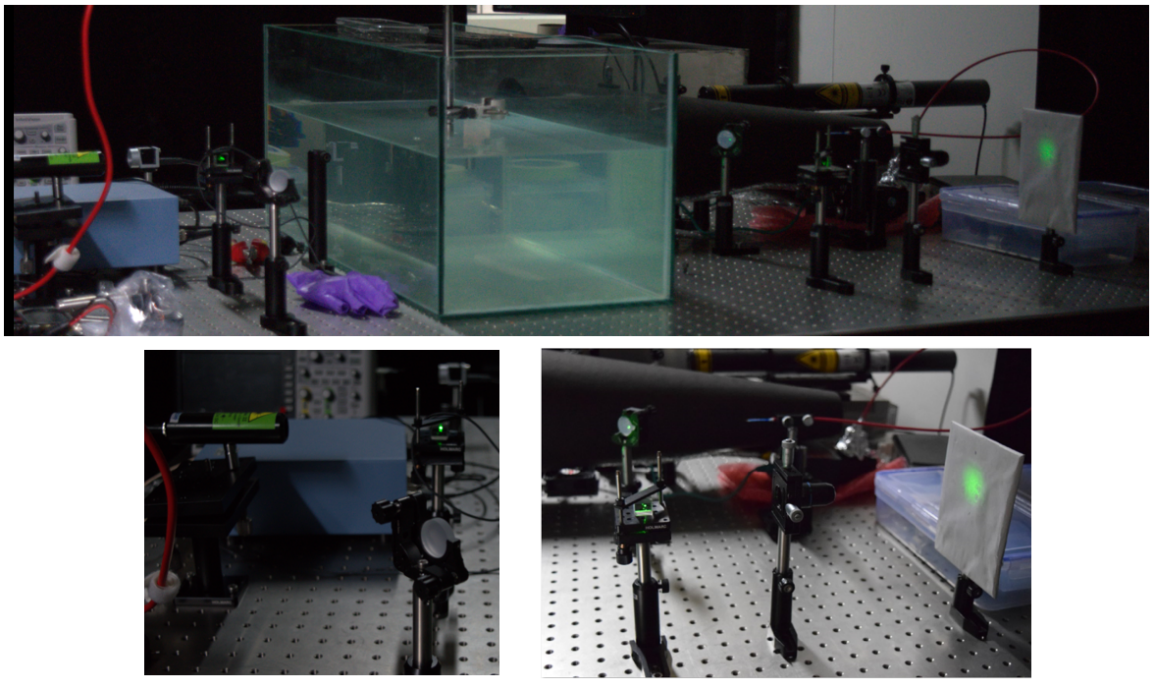

Figure 2.8: Experimental setup of the ultrasound detection using MZI.

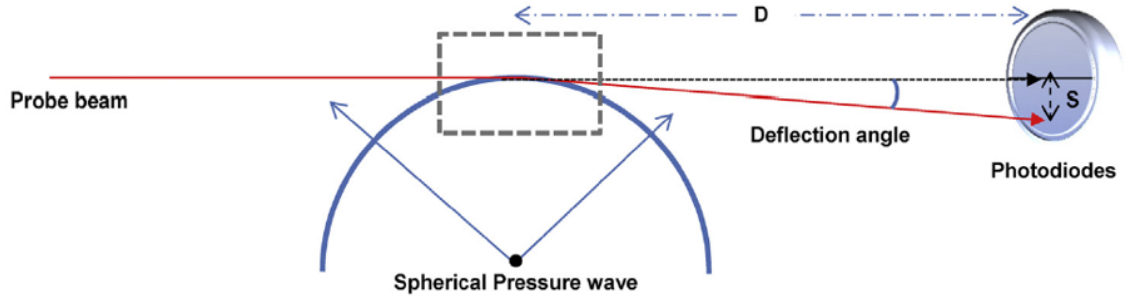

Figure 2.9: Detection of ultrasound by the deflection of a laser beam(reference-(MIR$^+$16))

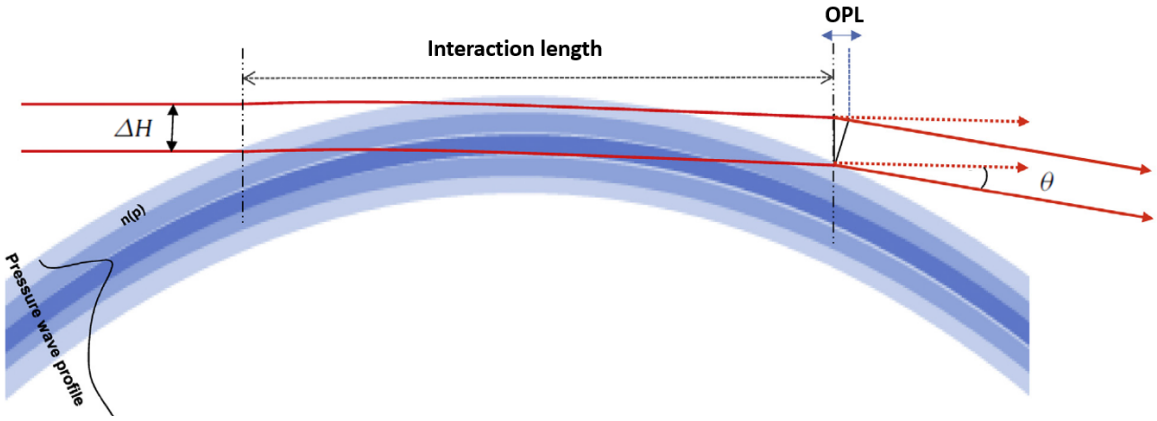

Figure 2.10: Schematic diagram of the interaction of probe beam and the ultrasound wave(reference-(MIR$^+$16)).

2.2 Detection of ultrasound by the deflection of a laser beam

According to the references-(MIR$^+$16), (PNHB07), (BMGS14) ultrasound can be detected by the deflection of the probe beam crossing the acoustic field(Figure-2.9). The acoustic waves change the refractive index of the medium and interact with the electric field of the probe laser beam and deflecting it in proportion to the pressure gradient of the acoustic wave(Figure-2.10). This deflection is detected using a position-sensitive detector, i.e. quadrant photodiode(QPD).

According to reference-(MIR$^+$16), a beam with a width of ΔH passing through a medium with a refractive index gradient as a function of pressure as shown in Figure-2.10. Due the pressure distribution, the refractive index distribution will be changed

and that can be approximated as $n(P) = n_m + \alpha P$, where α is the piezo-optic coefficient dn/dP of the medium (e.g. a for water is $1.35 \times 10^5\ bar^{-1}$) and n_m is the refractive index of the medium (e.g. water in this case). According to the Snell's law of refraction, when a light beam is moving from a rarer medium to the denser medium it bends towards the normal of the interface of two mediums. Due to this reason, we observe the deflection of the probe beam when it interacts with the ultrasound waves. The deflection angle of the probe beam can be formulated by the eq-(2.9),

$$\theta = \frac{L\ dn}{n_m\ \Delta H}\alpha P. \tag{2.9}$$

Where, L is the interaction length, dn refractive index modulation of the medium due to the ultrasound waves and P is the pressure profile of the ultrasound waves.

2.3 Ultrasound detection using inline Mach-Zehnder interferometer

In the previous sections, we have described two different experiments to detect the ultrasound waves. Here, we are going to describe an optical method of ultrasound waves detection. We have developed an inline Mach-Zehnder interferometer using a single wide beam. The schematic diagram of the experimental set up is given in Figure-2.11. Here, we have modified the free-space Mach-Zehnder interferometer by withdrawing one arm (reference beam). In the other arm is passing through the water medium. We have introduced an ultrasound wave in that arm. When the ultrasound passing through the beam some part of that beam will be affected by the ultrasound waves and another part of the same beam will not be affected. So, the unaffected part of the beam can be considered as a reference beam and the affected one is the object beam(see Figure-2.12). In this experimental setup, we have combined two optical methods for ultrasound detection one is *interference of light* and another one is *deflection of the light beam due to the ultrasound waves.*

According to the Figure-2.12, when the ultrasound waves reach the lower part of the laser beam, the beam starts to bend due to the Snell's law of refraction. So,

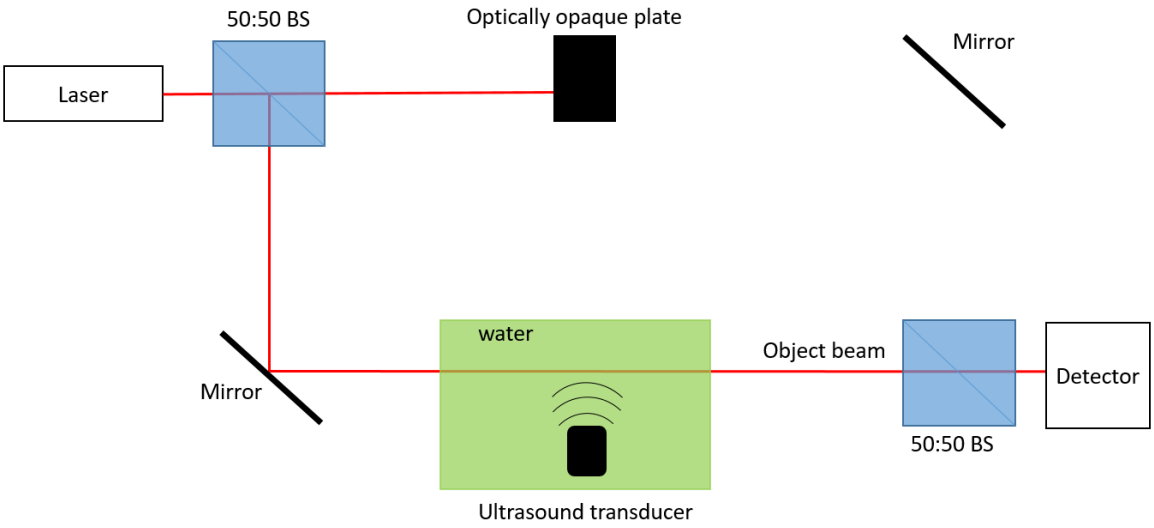

Figure 2.11: Schematic diagram of the inline Mach-Zehnder interferometer.

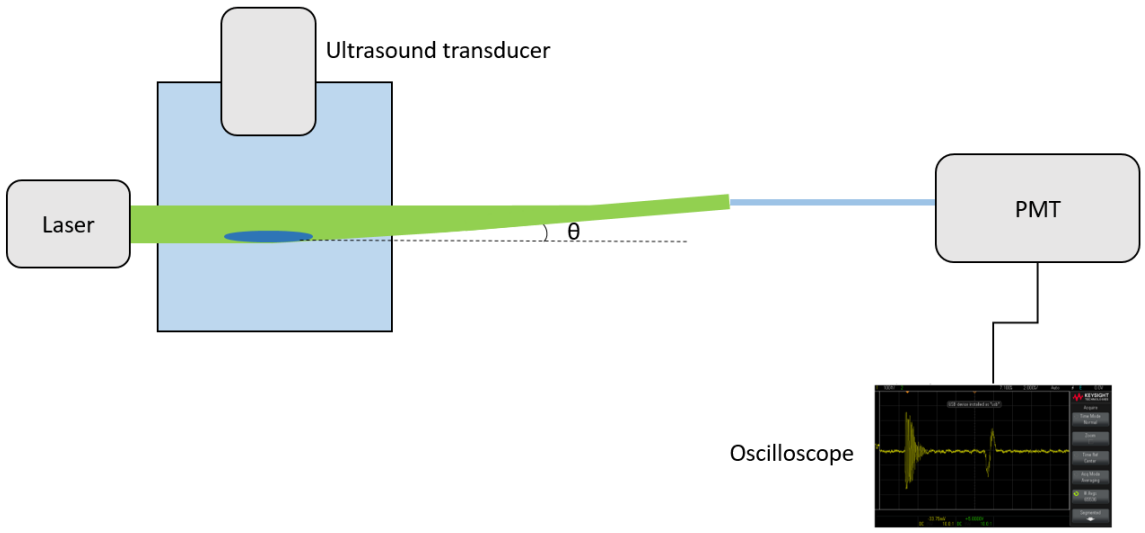

Figure 2.12: High frequency signal detection using optical methods.

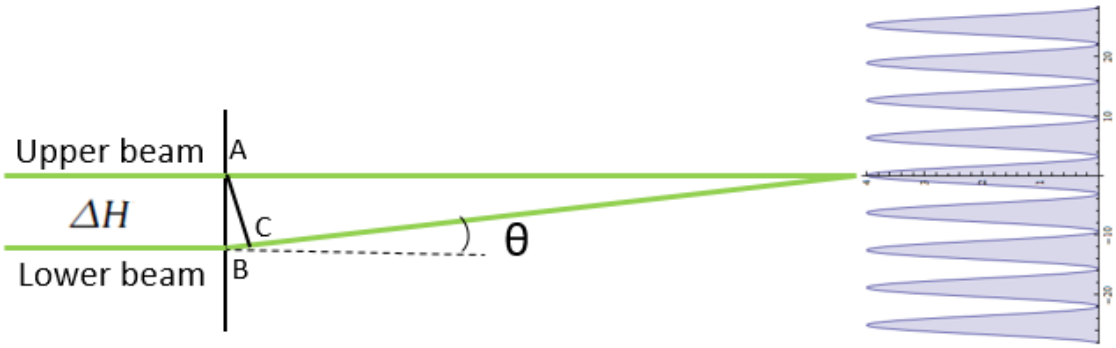

Figure 2.13: Schematic diagram of the interference formation.

there will be a path difference between the upper beam and the lower beam. Here, the upper beam is not affected by the ultrasound waves at that time because the upper beam is passing through the same refractive index. The upper beam acts as a reference beam and the lower one acts as an object beam. These two beams overlapped with each other and create an interference pattern. Due to the ultrasound wave propagation fringe shift is occurred at the output and that signal is transmitted through the 5mm optical fiber to the PMT. The PMT and the ultrasound transducer are connected with the oscilloscope. So, when the ultrasound interacts with the light some part of the ultrasound waves reflected back and detected by the transducer. The ultrasound signal due to the reflection is shown in the Figure-2.14(a). From this reflected ultrasound signal, we can say that the ultrasound wave interacts with the probe beam. If the interaction happens, the interference pattern should be formed and there should be an intensity fluctuation(sinusoidal carve) at the reflected ultrasound signal. The experimental proof of this concept is shown in the Figure-2.14(b). This phenomenon is observed only when the probe beam is wide(for our case the diameter of the beam spot is 3mm) enough. If we make a very narrow beam, the whole beam will be deflected, there will be no reference beam. So, there will be no interference pattern. The experimental proof of this concept is shown in the Figure-2.14(c).

The intensity distribution at the plane where the deflected beam and the reference beam are overlapped, is given in eq-(2.10),

$$I = I_1 + I_2 + 2\sqrt{I_1 I_2} cos(\phi) \tag{2.10}$$

where, I_1 is the intensity of the reference beam, I_2 is the intensity of the deflected beam and ϕ is the phase difference between two beams. In the previous section we showed the deflection angle which is,

$$\theta = \frac{L\ dn}{n_m\ \Delta H'} \alpha P \tag{2.11}$$

where, L is the interaction length, dn is the refractive index modulation due to the ultrasound waves, n_m is the refractive index of the medium, $\Delta H'$ is the width of the deflected beam, α is the piezo-optic coefficient and P is the pressure profile of the ultrasound wave.

According to the Figure-2.13, the width of the laser beam is ΔH. In the triangle ABC, angle BAC is θ. Therefore, $tan\theta = \frac{BC}{AB}$. The BC is the optical path difference(ΔOPL) between two beams. From the small angle approximation, we can say that $tan\theta \approx \theta$. Therefore,

$$\begin{aligned} \theta &= \frac{BC}{AB} = \frac{\Delta OPL}{\Delta H} \\ \Rightarrow \Delta OPL &= \Delta H \times \theta \\ \Rightarrow \Delta OPL &= \frac{L\ dn \Delta H}{n_m\ \Delta H'} \alpha P \end{aligned} \tag{2.12}$$

To measure the deflection angle we have measured the distance(D) between the tip of 1mm optical fiber and the ultrasound transducer and deflected length(S)[according to the Figure-2.9]. In our setup, first, we have found out the point where the reflected ultrasound signal strength is highest. Then measure the height of the 1mm optical fiber from the optical table. Then we have moved the 5mm optical fiber in the upward direction to find out that point where the signal vanishes. Similar way, we have found the location where the signal vanishes in the downward direction. Then, the deflection angle $\theta = tan^{-1}(S/D)$. In our experiment, the deflection angle is 0.0166°.

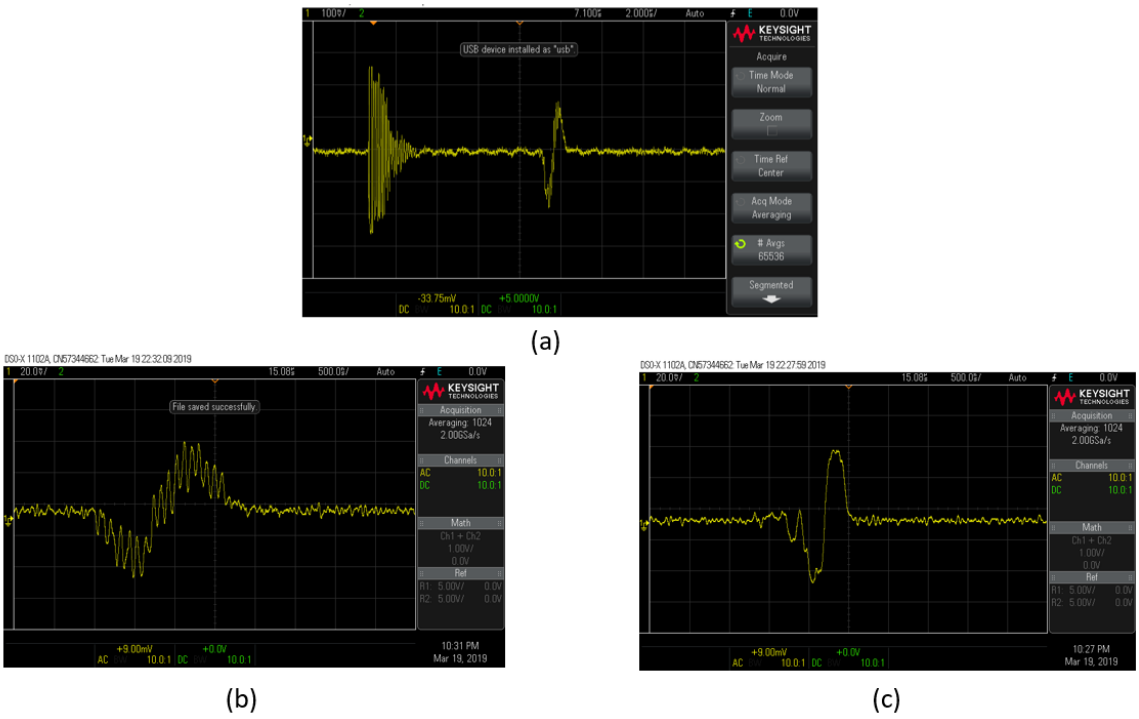

Figure 2.14: (a) Reflected ultrasound signal. (b) Intensity distribution due to the interference. (c)After reducing the beam width using $500\mu m$ pinhole, only reflected ultrasound signal is there.

Chapter 3

Optical fiber based Mach-Zehnder interferometer

To make a very compact and high sensitive sensor, we have tried to make a sensor using optical fiber. Here, we have used the optical fiber to create a Mach-Zehnder interferometer. Figure-3.1 is the schematic diagram of the experimental setup.

Here, one optical fiber is carrying a reference beam and the other one is carrying the object beam. In the object arm, we have created a $50 - 60\mu m$ cavity(see Figure-3.2) on the optical fiber and we have introduced ultrasound waves in that position. The ultrasound waves modulate the refractive index of the cavity medium. Due to this refractive index modulation, optical path length will be changed in the object arm. So, when we have combined the reference beam and the object beam we will see the fringe shift at the output. Without ultrasound waves, we have observed the interference pattern which is shown in Figure-3.2.

We have created such kind of micro-cavity using electric-arc based micro-machining system which is described in the later section.

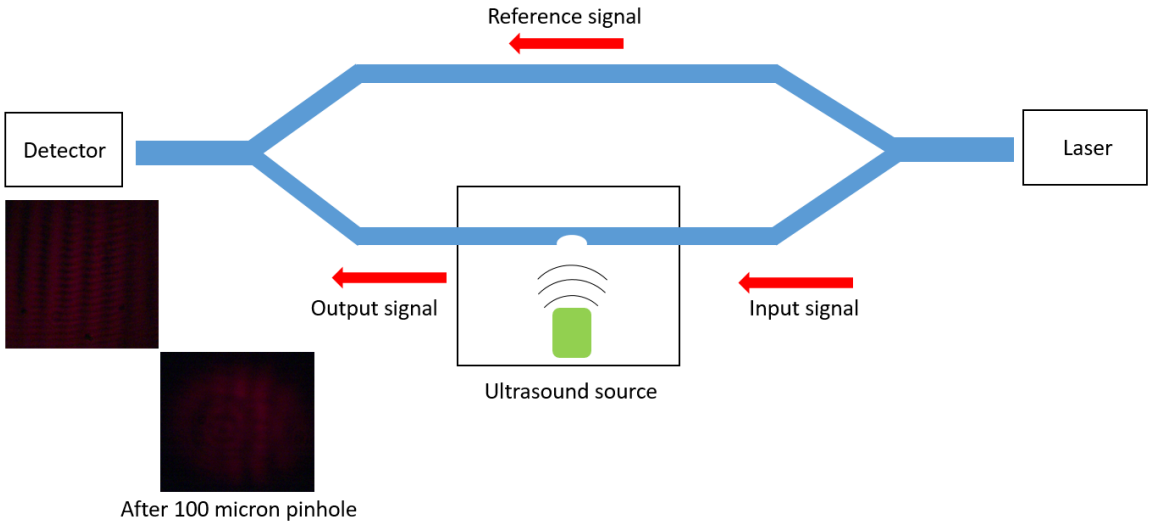

Figure 3.1: Schematic diagram of the optical fiber based Mach-Zehnder interferometer.

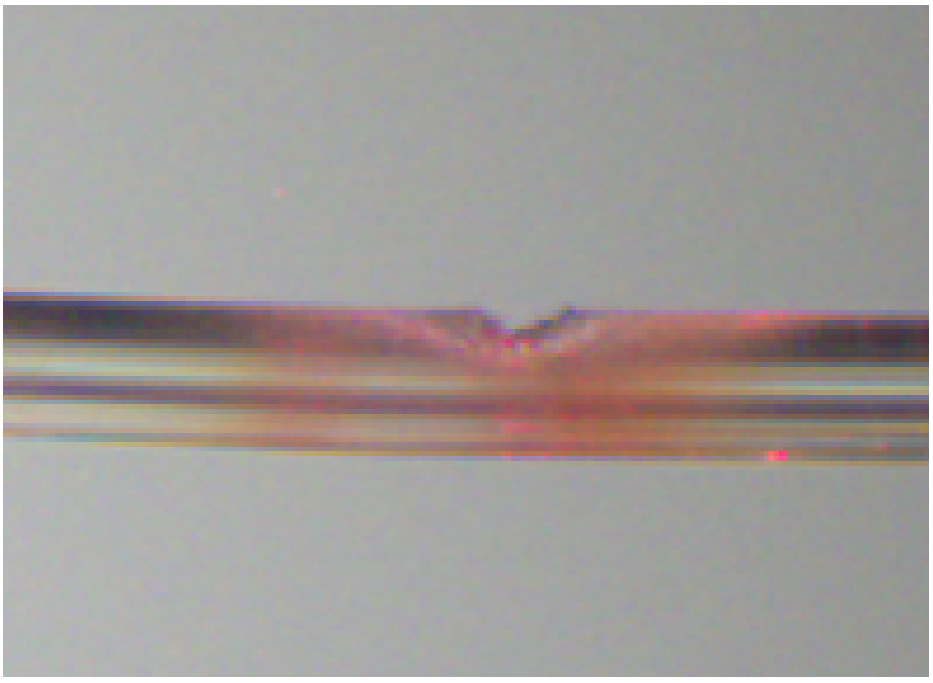

Figure 3.2: Micro-cavity on the optical fiber.

Chapter 4

Electric-arc based micro-machining system

People generally use the femtosecond lasers to create micro-cavity on the optical fiber. Those lasers are very costly, and lots of arrangements are needed to create a micro-machining system. Here, we have developed a low cost and very efficient micro-machining system. There are two electrodes one is cathode another one is an anode. The upper one is a cathode, and the lower one is an anode. A cathode is made of tungsten and anode is made of stainless steel. We have connected the anode with the high voltage power supply. The melting point of the tungsten is very high. To protect the cathode from the high temperature, we have chosen the tungsten material.

In that micro-machining system, we can do a lot of things on the optical fiber like micro-cavity, micro-sphere of different dimensions, even we can splice two optical fibers using that setup.

To observe the cavity condition, a microscope is attached with the micro-machining system. We have connected one end of the optical fiber with the laser to observe that the light is emitted from the cavity or not. As a side product, we have created the microspheres on the tip of the optical fiber(see Figure-4.4).

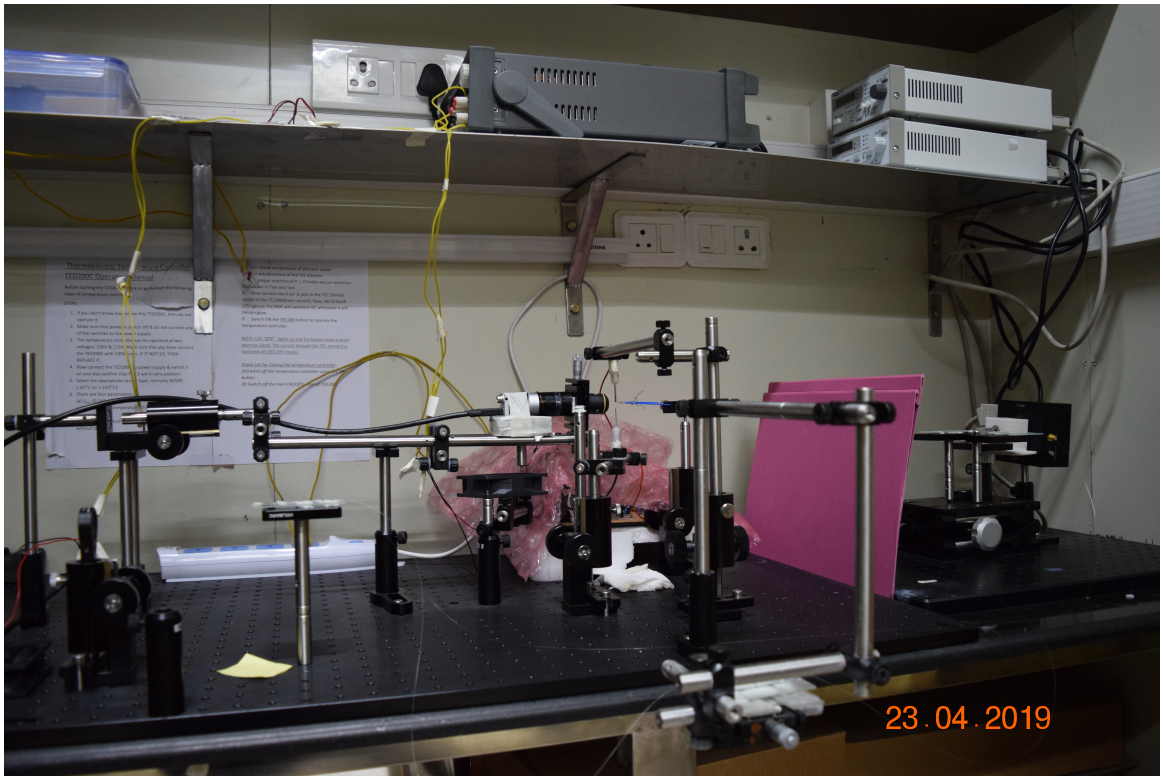

Figure 4.1: Electric-arc based micro-machining system.

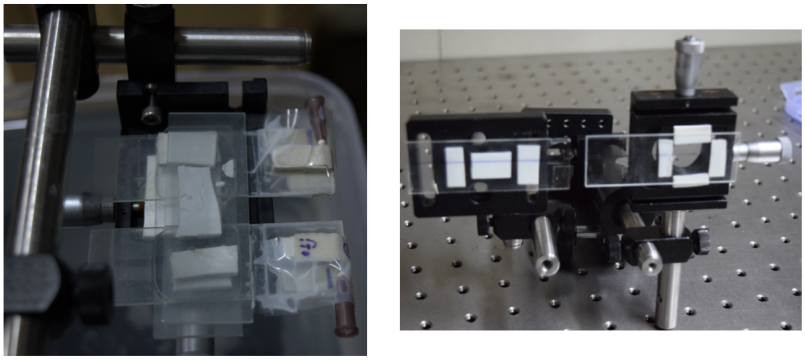

Figure 4.2: Different kind of optical fiber holders of the micro-machining system.

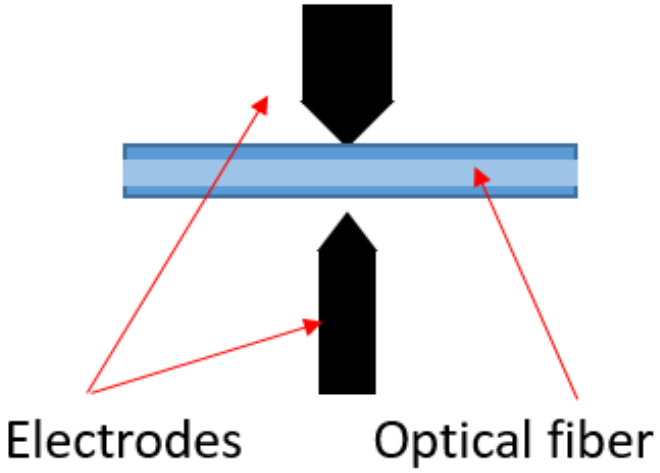

Figure 4.3: Procedure of cavity preparation.

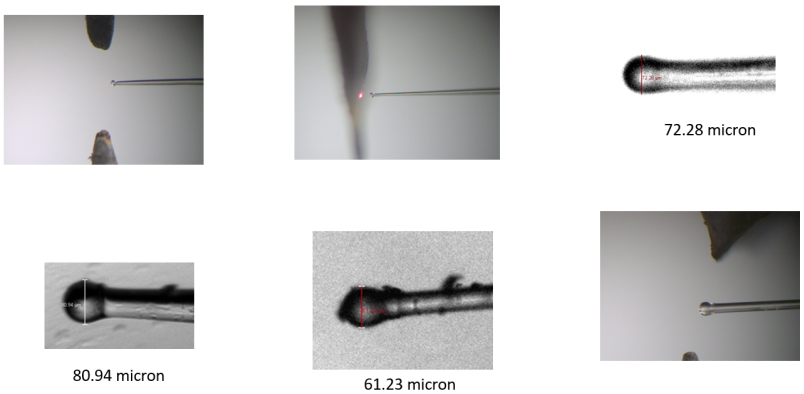

Figure 4.4: Micro-spheres using micro-machining system.

Chapter 5

Future plans

Using those micro-spheres we can reduce the laser beam spot size at the focal point of that micro-sphere. It can act as a lens. We can create the micro-lens array using such kind of microspheres. Besides this, we can develop an ultrasound wave detection setup using microspheres.

Bibliography

[BMGS14] Ronald A Barnes, Saher Maswadi, Randolph Glickman, and Mehdi Shadaram. Probe beam deflection technique as acoustic emission directionality sensor with photoacoustic emission source. *Applied optics*, 53(3):511–519, 2014.

[MIR+16] Saher M Maswadi, Bennett L Ibey, Caleb C Roth, Dmitri A Tsyboulski, Hope T Beier, Randolph D Glickman, and Alexander A Oraevsky. All-optical optoacoustic microscopy based on probe beam deflection technique. *Photoacoustics*, 4(3):91–101, 2016.

[PNHB07] Guenther Paltauf, Robert Nuster, Markus Haltmeier, and Peter Burgholzer. Photoacoustic tomography using a mach-zehnder interferometer as an acoustic line detector. *Applied optics*, 46(16):3352–3358, 2007.

[WPRN18] Georg Wissmeyer, Miguel A Pleitez, Amir Rosenthal, and Vasilis Ntziachristos. Looking at sound: optoacoustics with all-optical ultrasound detection. *Light: Science & Applications*, 7(1):53, 2018.